Energy band structure and linear optical properties of Si and Ge strained along the [111] and [110] directions

C. Tserbak and G. Theodorou*
Department of Physics, Aristotle University of Thessaloniki, 540 06 Thessaloniki, Greece
(Received 27 December 1994; revised manuscript received 30 May 1995)

The electronic and optical properties of Si and Ge coherently grown on (111) and (110) surfaces of $Si_{1-x}Ge_x$ alloy substrates are calculated with the use of a realistic empirical tight-binding model. The dependence of band-edge energies on strain and direction of growth is presented and the results are compared to those of the linear deformation potential theory. Nonlinear effects in the deformation potential theory are also considered for the conduction-band minima of Si along the Δ direction. The calculations show that these strained materials remain indirect gap semiconductors for all substrates and for both directions of growth. Their linear optical properties are analyzed in detail. Distortion along the [111] and [110] directions transforms the materials into uniaxial and biaxial crystals, respectively. The imaginary part of the dielectric function, $\varepsilon_2(\omega)$, along the principal axes is also calculated. The resulted anisotropy, as well as the structures in the ε_2 spectra, are analyzed in terms of the band structure and transition probabilities.

I. INTRODUCTION

Recent developments in advanced epitaxial techniques (molecular-beam epitaxy, metal-organic depositions, etc.) made the modification of the electronic properties of the Si-Ge system in a controlled way possible. The modification of strain, growth direction, and composition of $Si_{1-x}Ge_x$ alloy layers may produce materials with exciting properties appropriate for advanced device applications. Considerable theoretical and experimental work has been done in this direction.[1–4] The biggest part of this work has dealt with the properties of strained $Si_{1-x}Ge_x$ alloy layers, coherently grown on a $Si_{1-y}Ge_y(001)$ alloy surface.[5–9] People[5] has estimated the indirect gap of $Si_{1-x}Ge_x$ alloy layers coherently grown on a Si (001) substrate, with x in the range $0 \leq x \leq 0.75$, using linear deformation potential theory. More recently, Theodorou *et al.*[6] presented a theoretical study of structural, electronic, and optical properties of $Si_{1-x}Ge_x$ alloy layers grown on a Si(001) surface, for any alloy composition ($0 \leq x \leq 1$). Nonlocal empirical pseudopotential calculations have been done by Rieger and Vogl[7] in order to obtain realistic estimates for the effective masses, deformation potentials (DP), and band offsets for pseudomorphic $Si_{1-x}Ge_x$ alloy layers grown on $Si_{1-y}Ge_y$ (001) substrates.

The properties of strained $Si_{1-x}Ge_x$ alloy layers, grown on crystallographic planes other than (001), have not been extensively studied. Hinckley and Singh[10] have investigated the influence of strain and growth direction on the most significant near-band-edge properties, using a linear deformation potential theory. Ma *et al.*[11] have presented results for the band structure of strained $Si_{1-x}Ge_x$ alloy layers coherently grown on (001)-, (111)-, and (110)-oriented Si and Ge substrates, with the use of an empirical tight-binding method, and also made a systematic study of their symmetry properties. Their model describes well only the valence bands.

The objective of the present work is to investigate the electronic and optical properties of strained Si and Ge layers coherently grown on (111)- and (110)-oriented $Si_{1-x}Ge_x$ substrates. To our knowledge, this is the first time that the influence of strain along the [111] and [110] directions on the optical properties of Si and Ge layers is studied via a full-band structure calculation. Our calculations are based on a realistic tight-binding model that reproduces correctly both the valence and conduction bands in the entire Brillouin zone (BZ).[12] The modification by strain of the interaction parameters is taken into account in a way suitable to reproduce the experimental deformation potentials quite accurately. We have also calculated the main valence- and conduction-band-edge energies and compared them with the results of the phenomenological deformation potential theory. Finally, we have calculated the dielectric tensor for these materials and investigated its anisotropy, as well as the structures produced by strain in the imaginary part of the dielectric function, ε_2.

II. CRYSTAL STRUCTURE

For growth along the [111] and [110] directions, the knowledge of the strain tensor is not sufficient for the determination of the atomic positions in the unit cell. In addition, an internal displacement parameter ζ is needed for the determination of the position of the atoms.[13] Experimental as well as theoretical values for the parameter ζ are shown in Table I. We note that the theoretical predictions of Nielsen and Martin,[17] extracted from self-consistent total-energy calculations, are in agreement with the recently reported experimental values of the internal strain parameter,[16] while the calculations of Sanchez-Dehesa *et al.*[18] give Si results that are closer to

0163-1829/95/52(16)/12232(9)/$06.00

TABLE I. Theoretical and experimental values for the internal strain parameter ζ of Si and Ge.

ζ	Si	Ge
Exp.	0.74±0.04,[a] 0.72±0.04,[b] 0.54±0.04[c]	0.72±0.04[d], 0.54±0.04[c]
Theory	0.53,[e] 0.86[f]	0.44[e]

[a]D'Amour *et al.* (Ref. 14).
[b]Cousins *et al.* (Ref. 15).
[c]Cousins *et al.* (Ref. 16).
[d]Cousins *et al.* (Ref. 19).
[e]Nielsen and Martin (Ref. 17).
[f]Sanchez-Dehesa *et al.* (Ref. 18).

the older experimental values.[14,15] To clarify this point, we have done calculations for the internal strain parameter, using the empirical potential energy of Stillinger and Weber.[20,21] This model describes reliably the energetics of Si and Ge by using both two- and three-atom contributions. For small distortions, we get the values $\zeta(\mathrm{Si}) \simeq 0.63$ and $\zeta(\mathrm{Ge}) \simeq 0.51$ for both directions of growth. These values are close to the latest experimental measurements,[16] as well as to the theoretical results of Nielsen and Martin,[17] and will be used in the present calculations.

III. ELECTRONIC PROPERTIES

The empirical tight-binding (ETB) model of Ref. 12 will be used for the calculation of electronic and optical properties of strained Si and Ge. This model was extensively tested and it was found that it describes very well the most significant electronic and optical properties of bulk, as well as tetragonally (001) strained Si and Ge. The deformation potentials for tetragonal distortion along the [001] direction, calculated by this model, are in good agreement with the experimental values.[12] The influence of strain on the off-diagonal tight-binding parameters was evaluated by a scaling formula of the type

$$V_{\alpha\beta}(r) = V_{\alpha\beta}(r_0)\left(\frac{r_0}{r}\right)^{n_{\alpha\beta}} , \qquad (1)$$

where $V_{\alpha\beta}(r)$ and $V_{\alpha\beta}(r_0)$ are the strained and unstrained three center interaction parameters; r and r_0 the strained and unstrained interatomic distances; and $n_{\alpha\beta}$ the scaling indices that depend on the orbitals (α,β). These indices have been chosen so that the hydrostatic and uniaxial deformation potentials for distortions along the [001] and [111] directions are better reproduced. The resulted values for the indices are $n_{ss}=3$, $n_{sp}=1.8$, and $n_{pp}=1$. The calculated values for the DP's d and Ξ_u^L, as well as their experimental ones are given in Table II. At this point, it should be noted that the DP d depends in a quite sensitive way on the internal strain parameter ζ. A small increase in ζ results in a remarkable increase in the absolute value of d. For example, for $\zeta = 0.7$, it takes the value -4.8 for Si and -4.00 for Ge.

In this section, we will study the various energy states of strained, along the [111] and [110] directions, Si and Ge. The hydrostatic component of strain shifts the band edges without lifting their degeneracies, while the uniaxial one lifts the degeneracies. The important band edges in the Si-Ge system are the conduction-band minima in the Δ directions and at the L points, the valence-band maxima at Γ, labeled by V_1, V_2, and V_3, and the lowest conduction-band minimum at the Γ point, labeled by C_1. Uniaxial strain along the [111] direction splits the conduction-band minima at L points into two groups. The first group, $L(1)$, consists of the L state along the growth direction, while the second one, $L(3)$, of the remaining three L states. Strain along [110] direction splits the conduction-band minima both in the Δ directions and at the L points. The conduction-band minima along the Δ directions split into two groups with degeneracies two and four, denoted by $\Delta(2)$ and $\Delta(4)$, respectively. The first group consists of the states along the two equivalent $\langle 001\rangle$ directions and the second of the four states along the $\langle 100\rangle$ directions. The conduction-band minima at the L points also split into two groups. The first group, $L_1(2)$, consists of the two L-point states along the directions [111] and $[11\bar{1}]$, and the second one, $L_2(2)$, of the remaining two L-point states along the directions $[\bar{1}11]$ and $[1\bar{1}1]$.

TABLE II. Calculated and experimental deformation potentials (in eV) for Si and Ge.

	Si		Ge	
	Exp.	Theory	Exp.	Theory
d	-5.3±0.4,[a] -4.85±0.15[b]	-4.04,[c] -5.32[d]	-5.28±0.5,[a] -5.0[e]	-2.83,[c] -5.50[d]
Ξ_u^L		14.75,[c] 16.14[d]	16.2±0.4[b]	11.94,[c] 15.13[d]

[a]Balslev (Ref. 24).
[b]Laude *et al.* (Ref. 23).
[c]Present work.
[d]Van de Walle and Martin (Ref. 25).
[e]Cardona and Harbeke (Ref. 26).

A. Strain along the [111] direction

In Fig. 1 are shown the calculated energies, using the ETB model, for the valence-band maxima (V_1, V_2, V_3) and the conduction-band minima (in the Δ directions and at the L points), as a function of x, for strained Si (s-Si) and strained Ge (s-Ge), coherently grown on a $Si_{1-x}Ge_x(111)$ alloy surface. In the same figure are also shown the results for the L point and V_1, V_2, V_3 state energies calculated from the linear deformation potential theory[22,23] and the experimental values of the deformation potentials. The agreement between these two calculations is very good.

The nonlinear effects that may occur in the deformation potential theory are generally small and usually are not taken into account. However, in some cases, and, in particular, for relatively large values of strain, these effects are significant and cannot be ignored. For example, the conduction-band degeneracy at the X point of the bulk Si and Ge BZ is lifted under uniaxial strain. However, the resulting splitting cannot be explained by the use of linear deformation potential theory. Laude, Pollak, and Cardona[23] have described this splitting with the introduction of a nonlinear shear deformation potential ϵ_2^*. This nonlinear potential produces a shift in the Δ_1 conduction-band minima, which to second order in stress is given by

$$\delta E^*(\Delta) = -\frac{(2\epsilon_2^*\epsilon_{xy})^2}{E(\Delta_{2'}) - E(\Delta_1)}, \tag{2}$$

where $E(\Delta_1)$ and $E(\Delta_{2'})$ are the energies, in increasing order, of the two lowest conduction-band states at the position of the conduction-band minimum in the bulk materials. This shift becomes quite sizable for large strain and cannot be ignored. The total variation in energy for the $\Delta(6)$ states of Si, for which experimental data for ϵ_2^* are available[23] ($\epsilon_2^* = 8.0$), including both the linear and nonlinear terms in the deformation potential theory, is given in Fig. 1(a). Even with the inclusion of this nonlinear term, there is for the conduction-band minimum along the Δ direction a large deviation between the results of the ETB model and those of the deformation potential theory. This discrepancy is mainly due to the fact that the ETB model does not reproduce correctly the DP $\left(\Xi_d^\Delta + \frac{1}{3}\Xi_u^\Delta\right) - a^v$.[12] From these results, we get that for Si strained along the [111] direction, the conduction-band minimum always remains along the Δ direction (ΓF direction in the distorted BZ). The respective indirect gap decreases appreciably as the distortion increases. The direct gap at the Γ point also decreases with the distortion and takes the value of 2.70 eV for s-Si grown on a Ge(111) substrate.

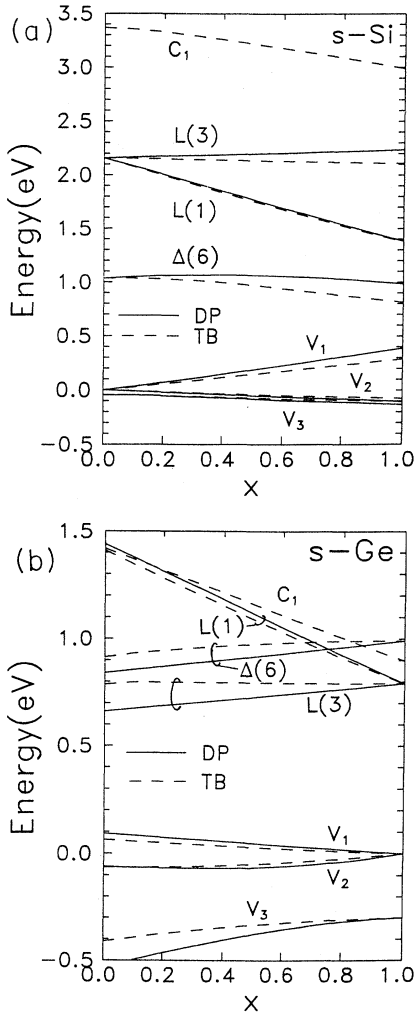

FIG. 1. Valence-band maxima at the Γ point (V_1, V_2, V_3) and conduction-band minima along the Δ direction and at L points, as a function of x, for (a) strained Si, and (b) strained Ge coherently grown on a $Si_{1-x}Ge_x$ (111) substrate. Solid lines represent results from the deformation potential theory and dashed lines represent the calculated values from the ETB model of the present work.

The variation in energy of the $\Delta(6)$ states for s-Ge according to the linear deformation potential theory, is given in Fig. 1(b). For s-Ge, the conduction-band minimum appears at the Z point of the distorted BZ. The respective indirect gap decreases with the increase of the distortion. On the contrary, the direct gap at the Γ point increases from the value of 0.9 eV for bulk Ge to 1.36 eV for s-Ge coherently grown on a Si(111) substrate.

The band structures of s-Si grown on a Ge(111) substrate and of s-Ge grown on a Si(111) substrate are shown in Fig. 2. The anisotropy between the bands along the ΓZ and ΓL directions is clear. This is connected to the fact that the group of $\mathbf{k}$ vectors along the ΓZ direction and the corresponding irreducible representations remain the same as in the unstrained materials, while the symmetry along the ΓL direction reduces with strain. The six $\langle 100 \rangle$ directions remain equivalent in the distorted case, but their symmetry is reduced. For s-Si grown on a $Si_{1-x}Ge_x(111)$ substrate, the top two valence bands along the ΓL direction exhibit an almost constant splitting, which increases with x and takes the value of about 0.4 eV for $x = 1$. On the contrary, parallel to the ΓZ direction, this splitting is quite small ($\sim$ 0.03 eV) and independent of the distortion. Similar behavior is also

seen for the case of s-Ge. For $x = 1$, the splitting of the top two valence bands along ΓZ is 0.2 eV and 0.36 eV along the ΓL direction.

The fourfold degeneracy of the states at the X point of the bulk Si and Ge (becoming the F point of the distorted BZ) is lifted with strain. These states split into two twofold-degenerate states with even and odd parity, respectively. The splitting has a nonlinear origin and is larger for the two lowest conduction-band states. For s-Si grown on a Ge (111) substrate takes the value of $\Delta E_{\rm NL} = 0.67$ eV, while for s-Ge grown on a Si (111) substrate it becomes 0.53 eV.

B. Strain along the [110] direction

Figure 3 shows the variation of the band-edge energies for s-Si and s-Ge coherently grown on a $Si_{1-x}Ge_x(110)$ alloy substrate. As previously mentioned, strain along the [110] direction lifts the degeneracy of the six equivalent $\langle 100 \rangle$ directions for the undistorted bulk materials. For s-Si, linear deformation theory predicts that the $\Delta(2)$ states always lie higher than the $\Delta(4)$ states. However, the inclusion of the nonlinear term, Eq. (2), modifies the ordering as follows:

$$E(\Delta(2)) > E(\Delta(4)) \quad \text{for} \quad x < 0.5$$

and

$$E(\Delta(2)) < E(\Delta(4)) \quad \text{for} \quad x > 0.5.$$

The ETB model predicts that for s-Si, the $\Delta(2)$ state is the global minimum of the conduction band for every value of x. This discrepancy is again due to the failure of the ETB model to reproduce the correct value of the DP $(\Xi_d^{\Delta} + \frac{1}{3}\Xi_u^{\Delta}) - a^v$. For the valence and the remaining conduction-band states the two calculations agree very well. For the case of s-Ge, the global minimum of the conduction-band remains, for every value of x, the $L_1(2)$ states (along the directions [111] and [11$\bar{1}$]), and for growth on a Si(110) substrate it almost coincides with the $\Delta(2)$ local minimum.

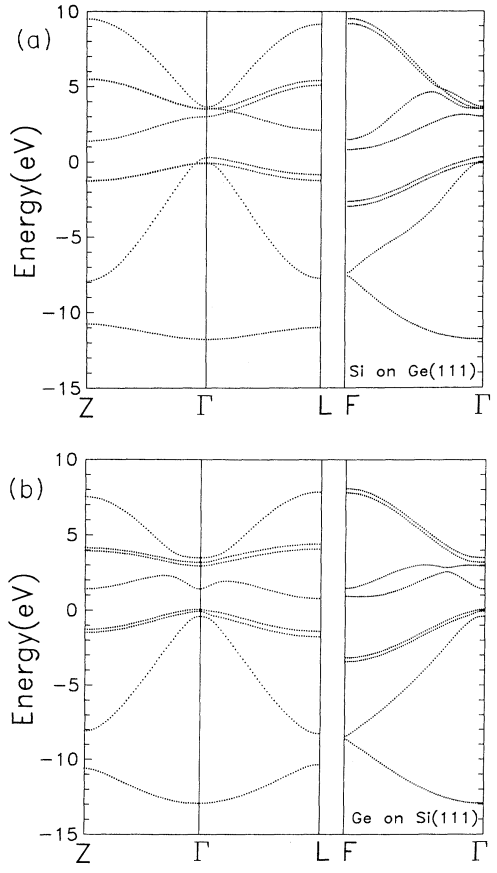

FIG. 2. The band structure of (a) strained Si, coherently grown on a Ge(111) substrate, and (b) strained Ge, coherently grown on a Si(111) substrate.

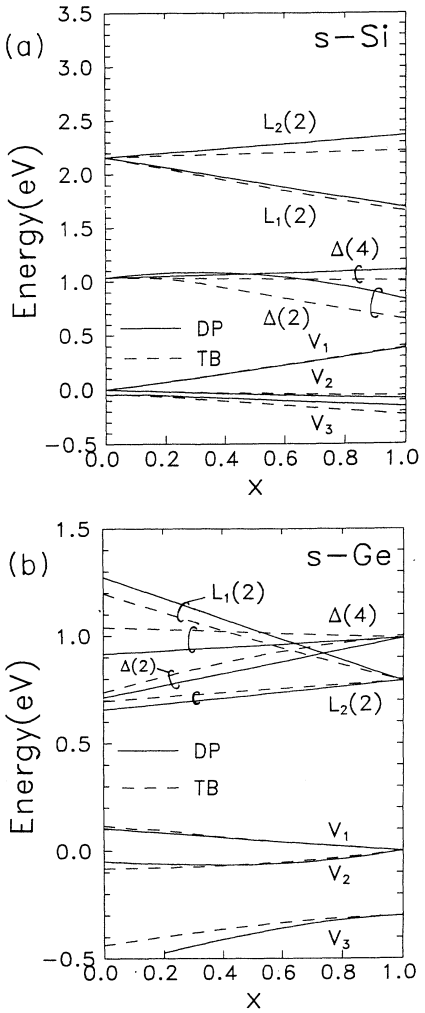

FIG. 3. Valence-band maxima at the Γ point (V_1, V_2, V_3) and conduction-band minima along the Δ direction and at L points, as a function of x, for (a) strained Si, and (b) strained Ge, coherently grown on a $Si_{1-x}Ge_x$ (110) substrate. Solid lines represent results from deformation potential theory and dashed lines the calculated values from the ETB model of the present work.

IV. OPTICAL PROPERTIES

We investigate the effect of strain on the optical properties of Si/Ge. For this purpose, we calculate the imaginary part, $\varepsilon_2(\omega)$, of the dielectric function.[27]

A. Si strained along the [111] direction

For growth on a (111)-oriented substrate surface, the symmetry is rhombohedral and the crystal uniaxial. In Fig. 4 are shown the components of ε_2 parallel and perpendicular to the growth plane for s-Si grown on a Ge (111) surface. The important point to notice in this figure is the strong anisotropy between these two components from the absorption edge up to about 4.5 eV. For larger energies, this anisotropy is small. In addition, the onset energy appears to be different, 2.63 eV in $\varepsilon_2^{\parallel}$ and ~ 3.0 eV in $\varepsilon_2^{\perp}$. This behavior can be explained in terms of the band structure of Fig. 1(a), and the transition probabilities at the points Γ, Z, L, and F, shown in Table III. The minimum direct transition energy, equal to 2.63 eV, appears at the Z point of the distorted BZ, coinciding with the onset in $\varepsilon_2^{\parallel}$. This transition is polarized in the growth plane. The direct transitions contributing to ε_2 below 3 eV are those between the two upper valence bands (V_1, V_2) and the lowest conduction band (C_1), close to the Z point and parallel to the ΓZ direction of the strained BZ. The probabilities for these transitions, on the other hand, have significant values only for polarization parallel to the growth plane and are almost zero for polarization perpendicular to it. This explains the result that $\varepsilon_2^{\perp} \approx 0$ for energies between 2.63 and 3 eV. For larger energies, transitions along the ΓL direction start to contribute to ε_2. At the L point, the lowest transitions, $V_1 - C_1$ and $V_2 - C_1$, occur at 2.95 and 3.34 eV, respectively, with significant transition probabilities for both polarizations. The steplike behavior of $\varepsilon_2^{\perp}$ close to 3 eV comes from these latter transitions.

The most pronounced structure in ε_2 is the E_2-like peak. The position of this peak, as well as its width, differ significantly for the two polarizations, being a sharp structure in $\varepsilon_2^{\perp}$ and a broad one in $\varepsilon_2^{\parallel}$. To explain this behavior, we are going to investigate the transitions responsible for the E_2 structure. For the case of bulk Si, the transitions responsible for the E_2 structure are between the top valence- and lowest conduction-band states in a region near to the X point. For Si strained along the [111] direction, the X_5 fourfold-degenerate states of bulk Si are split into two twofold-degenerate states with opposite parity, at the F point of the distorted BZ. The optical transitions $V_2 - C_1$ and $V_1 - C_2$, close to the F point, with transition energies at 3.77 and 4.1 eV, respectively, have appreciable transition probabilities for polarization in the growth plane. On the other band, for polarization perpendicular to the growth plane, only transition $V_1 - C_2$ exhibits significant transition probability. This behavior accounts for the broad E_2-like peak in $\varepsilon_2^{\parallel}$ and the sharp one in $\varepsilon_2^{\perp}$.

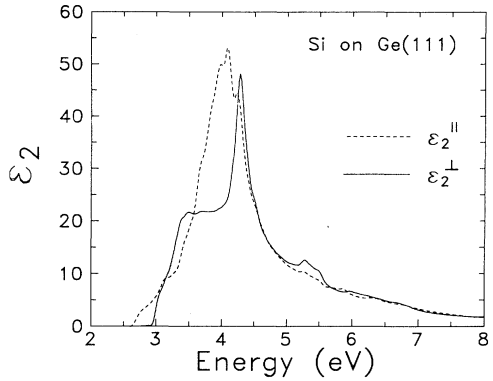

FIG. 4. Imaginary part of the dielectric function, ε_2, of strained Si, grown on a Ge(111) substrate, for polarization parallel ($\varepsilon_2^{\parallel}$) and perpendicular ($\varepsilon_2^{\perp}$) to the growth plane.

In Fig. 5 are shown the transition energies at points Γ, Z, L, and F, for transitions responsible for the main structures in ε_2, as a function of strain. We point out the following: (i) The onset in ε_2 always comes from transitions at the Z points, whose transition energies get

TABLE III. Transition probabilities, in units of $(h/a)^2$, for Si and Ge coherently grown on a Ge(111) and Si(111) surface, respectively.

Material	Polarization	Transition	Γ	Z	L	F
s-Si	$[\bar{1}10]$	$V_1 - C_1$	4×10^{-3}	1.0	0.2	0
		$V_2 - C_1$	0.9	1.0	0.6	0.9
		$V_1 - C_2$	0	1.3	0.1	1.
	[111]	$V_1 - C_1$	0.5×10^{-1}	0	1.6	0
		$V_2 - C_1$	0	2×10^{-6}	2×10^{-3}	2×10^{-6}
		$V_1 - C_2$	0	0	1.3	2
s-Ge	$[\bar{1}10]$	$V_1 - C_1$	0.9	1.1	0.4	0
		$V_2 - C_1$	0.7	1.1	0.2	0.7
		$V_1 - C_2$	0	0.7	0.1	0.7
	[111]	$V_1 - C_1$	0	0	0.2	0
		$V_2 - C_1$	0.6	2×10^{-6}	1.9	2
		$V_1 - C_2$	0	0	0.7	2×10^{-5}

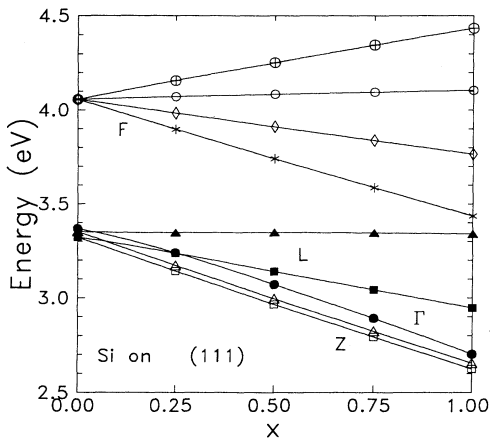

FIG. 5. Transition energies at the symmetry points Γ, Z, L, and F of strained Si coherently grown on a $Si_{1-x}Ge_x$ (111) substrate, as a function of x. The results represent (a) the lowest transition at Γ point (full circle); (b) the two lowest transitions, $V_1 - C_1$ ($\Box$) and $V_2 - C_1$ ($\triangle$), at Z point; (c) the two lowest transitions, $V_1 - C_1$ (full squares) and $V_2 - C_1$ (full triangles), at L point; and (d) the four lowest transitions, $V_1 - C_1$ ($\star$), $V_2 - C_1$ ($\Diamond$) , $V_1 - C_2$ ($\bigcirc$), and $V_2 - C_2$ ($\oplus$), at F point.

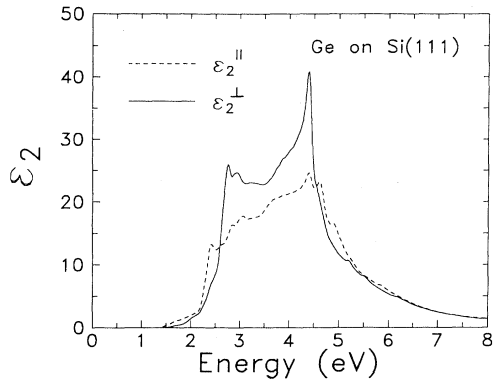

FIG. 6. Imaginary part of the dielectric function, ε_2, of strained Ge grown on a Si (111) substrate for polarization parallel ($\varepsilon_2^{||}$) and perpendicular ($\varepsilon_2^{\perp}$) to the growth plane.

smaller as strain increases. (ii) The transition energy for the lowest transition at the L point, $(V_1 - C_1)$, decreases with strain, while for the next one, $(V_2 - C_1)$, remains almost strain independent. (iii) The transitions between the highest valence and lowest conduction bands at the X point of the unstrained BZ split with strain into four components. Among these four transitions, $V_1 - C_2$ and $V_2 - C_1$ exhibit significant transition probabilities, with $V_2 - C_1$ polarized almost in the growth plane. The energy for the transition $V_2 - C_1$ reduces with strain, while for the $V_1 - C_2$ one has a minor variation. This behavior explains the result that the energy of the E_2- peak in $\varepsilon_2^{\perp}$ is almost strain independent, while in $\varepsilon_2^{||}$ reduces with strain with a corresponding increase in its width.

B. Ge strained along the [111] direction

Figure 6 shows the components of ε_2 for s-Ge grown on a Si(111) surface. There again exists a strong anisotropy in the region between 2.5 and 4.5 eV, with $\varepsilon_2^{\perp} > \varepsilon_2^{||}$. For energies larger than 4.5 eV, this anisotropy is quite small, as in the case of s-Si. The onset in $\varepsilon_2^{||}$ coincides with the direct gap at Γ, equal to $E_g^{\Gamma} = 1.36$ eV, while in $\varepsilon_2^{\perp}$ appears at higher energies, $\simeq$1.48 eV. This occurs because the lowest transition at Γ, $V_1 - C_1$, is polarized along the growth plane, as shown in Table III.

It is well known that for bulk Ge the E_1 structure in ε_2 is due to transitions between the parallel bands along the Λ direction and close to the L point. The parallel structure of the bands also remains in the case of s-Ge, but the L point of the BZ splits with strain into two nonequivalent points, Z and L. This splitting makes the E_1 structure more extended. The energies of the two lowest transitions at the L point of the strained BZ, $V_1 - C_1$ and $V_2 - C_1$, are equal to 2.18 and 2.54 eV, respectively, with the transition probability for the $V_2 - C_1$ transition and polarization perpendicular to the growth plane one order of magnitude larger than that for polarization in the growth plane. For these reasons, the E_1 structure in $\varepsilon_2^{\perp}$ exhibits larger values. At the Z point, the energies for two lowest transitions are equal to 2.70 and 2.90 eV, and essentially polarized in the growth plane.

The E_2 structure in ε_2 appears around 4.5 eV. The E_2 peak in $\varepsilon_2^{\perp}$ is quite strong and sharp, while in $\varepsilon_2^{||}$ has almost half the strength with a considerably larger width and is split into two peaks. The transitions responsible for the E_2 structure in bulk Ge take place in a region around the XU direction.[12] For strain along the [111] direction, the bulk fourfold degenerate states at X_5 split into two twofold degenerate states with opposite parity. For polarization in the growth plane, the main contribution to E_2 structure comes from both $V_2 - C_1$ and $V_1 - C_2$ transitions whose energies are equal to 4.35 and 4.63 eV, respectively, implying a double peak structure in ε_2 for this polarization. For polarization perpendicular to the growth plane, the main contribution comes only from the $V_2 - C_1$ transitions, with a transition probability three times larger than that for parallel polarization. These results explain the sharp and strong peak in $\varepsilon_2^{\perp}$.

In Fig. 7 are shown the transition energies at points Γ, Z, L, and Γ, for transitions responsible for the main structures in ε_2, as a function of strain. The absorption edge is due to transitions at Γ and its energy increases with strain, that is with a reduction of the concentration x of Ge in the substrate. The difference in energy between the two lowest transitions at L, as well as at the Z point, increases with strain. The transition energy for the transition $V_2 - C_1$ is almost strain independent, while for the $V_1 - C_2$ transition increases with strain, implying that the energy position and width of the E_2 structure are strain independent in $\varepsilon_2^{\perp}$, while increasing with strain in $\varepsilon_2^{||}$.

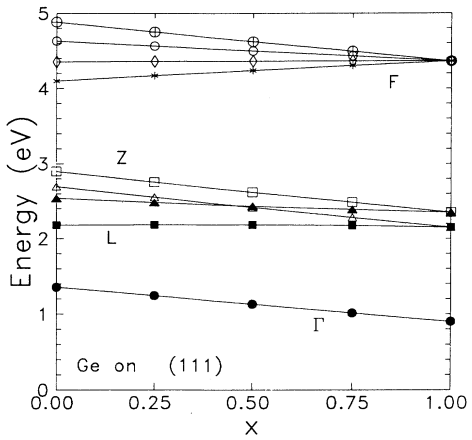

FIG. 7. Transition energies at the symmetry points Γ, Z, L, and F of strained Ge coherently grown on a $Si_{1-x}Ge_x$ (111) substrate, as a function of x. The notation is the same as in Fig. 5.

C. Si strained along the [110] direction

The crystal in this case is biaxial, with three independent components of the dielectric tensor. Figure 8 shows the three components of the imaginary part of the dielectric tensor along the three principal axes, for *si*-Si grown coherently on a Ge(110) surface. The smallest direct gap appears at Γ and is equal to $E_g^\Gamma = 2.64$ eV. As can be seen from Fig. 9, the onset in all components of ε_2 appears at slightly higher energies, where the transitions between the parallel bands along the ΓR direction, close to the R point, of the BZ start to contribute significantly. At the R point, the energies of the two lowest transitions are equal to 2.78 and 2.89 eV. At even slightly higher energies, the contribution from the transitions along the ΓS direction close to the S point of the BZ starts. The lowest transition energies at this point are 2.94 and 3.52 eV.

The transitions along the ΓR and ΓS directions are

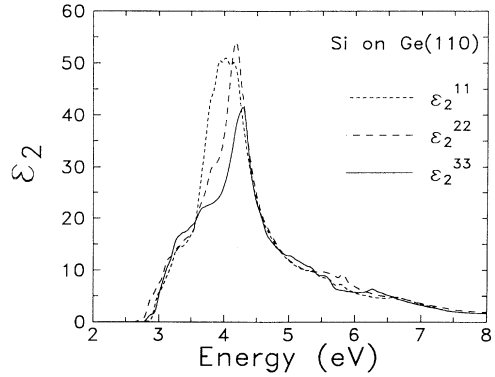

FIG. 8. Imaginary part of the dielectric function, ε_2, of strained Si coherently grown on a Ge (110) substrate for polarizations along the principal axes $[\bar{1}10]$ (ε_2^{11}), [001] (ε_2^{22}), and [110] (ε_2^{33}).

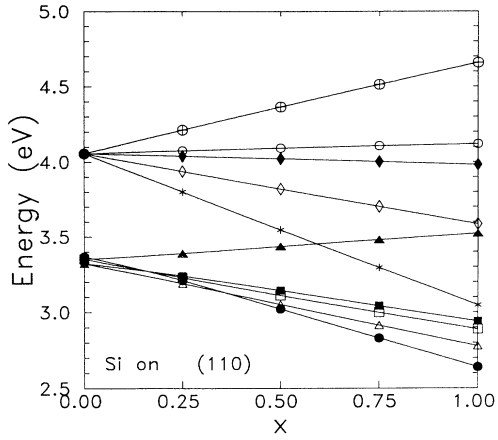

FIG. 9. Transition energies at the symmetry points Γ, S, R , T, and X of strained Si coherently grown on a $Si_{1-x}Ge_x$ (110) substrate, as a function of x. The results represent (a) the lowest transition at Γ point (full circle); (b) the two lowest transitions, $V_1 - C_1$ (△) and $V_2 - C_1$ (□), at S point; (c) the two lowest transitions, $V_1 - C_1$ (full squares) and $V_2 - C_1$ (full triangles), at R point; (d) the four lowest transitions, $V_1 - C_1$ (⋆), $V_2 - C_1$, (◇) , $V_1 - C_2$ (○) and $V_2 - C_2$ (⊕), at X point; and (e) the lowest transition at the T point (full diamonds).

responsible for the E_1-like structure in ε_2. The E_1 structure exhibits a small anisotropy. The strong anisotropy happens in the region between 3.5–4.2 eV, where the E_2-like structure is located. The E_2 peak has the smallest strength as well as width in the ε_2^{33} component. The transitions responsible for the E_2 structure take place in regions close to the points T and X of the distorted BZ. The anisotropy of the bands near these points, as well as the different behavior of the transition probabilities for different polarizations, produce the strong anisotropy of the E_2 structure.

In Fig. 9 are shown energies for the lowest transitions at points Γ, S, R, T, and X of the distorted BZ, as a function of strain. The absorption edge in ε_2 is due to transitions at R point for concentrations x of Ge in the substrate smaller than 0.3, while for $x > 0.3$ to transitions at Γ. The difference in energy between the two lowest transitions at R, as well as at S, increases with strain. This splitting is larger for the S point. Among the lowest four transitions at X point, only $V_2 - C_1$ and $V_1 - C_2$ transitions have significant transition probabilities. Their splitting increases with strain. The lowest four transitions at T are practically strain independent.

D. Ge strained along the [110] direction

In Fig. 10 are shown the three components of $[\varepsilon_2]$ tensor, along the three principal axes, of *s*-Ge grown coherently on a Si(110) surface. The orthorhombic anisotropy is large in the range from the absorption edge up to the E_2 structure. For energies smaller than ~ 2.5 eV, the ordering of the components of the dielectric tensor is $\varepsilon_2^{11}, \varepsilon_2^{22} > \varepsilon_2^{33}$, while for energies in the region 2.5–4.5 eV, ε_2^{11}, $\varepsilon_2^{22} < \varepsilon_2^{33}$. The absorption edge coincides with

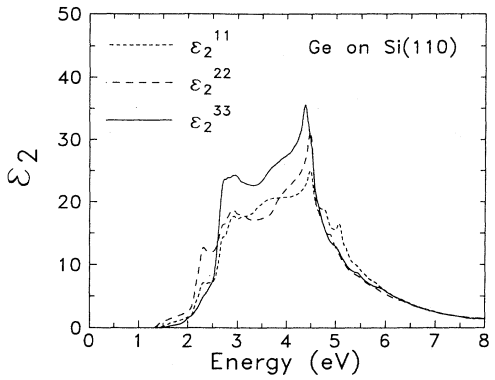

FIG. 10. Imaginary part of the dielectric function, ε_2, of strained Ge coherently grown on a Si (110) substrate for polarizations along the principal axes [$\bar{1}$10] (ε_2^{11}), [001] (ε_2^{22}), and [110] (ε_2^{33}).

the direct gap at Γ, equal to E_g^{Γ}=1.27 eV. The tail in ε_2, up to $\sim$ 2 eV, is due to transitions around the Γ point. At energies larger than 2 eV, the significant contribution from the directions ΓS and ΓR near the R and S points starts to take effect. These transitions are responsible for the E_1 structure. The E_2 peaks exhibit a strong anisotropy, for reasons similar to Si strained along the [110] direction. Finally, in Fig. 11 are shown the transition energies of the lowest transitions at points Γ, S, R, X, and T as a function of strain.

E. Static dielectric constant

We have also calculated the interband contribution to the static dielectric constant $\varepsilon_1(0)$, by the use of the Kramers-Kronig relation.[28] The results are presented in Figs. 12 and 13 for s-Si and s-Ge, coherently grown on (111)- and (110)-oriented $Si_{1-x}Ge_x$ substrates. For light polarization perpendicular to the growth plane the static

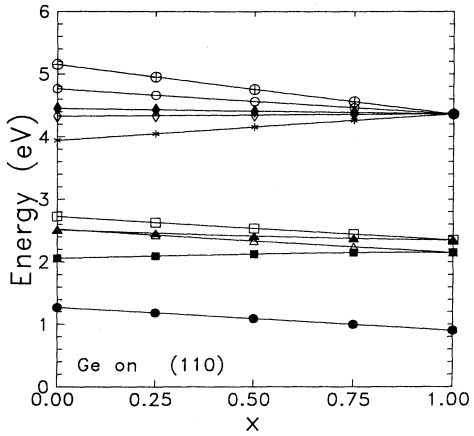

FIG. 11. Transition energies at the symmetry points Γ, S, R, T, and X of strained Ge coherently grown on a $Si_{1-x}Ge_x$ (110) substrate, as a function of x. The notation is the same as in Fig. 9.

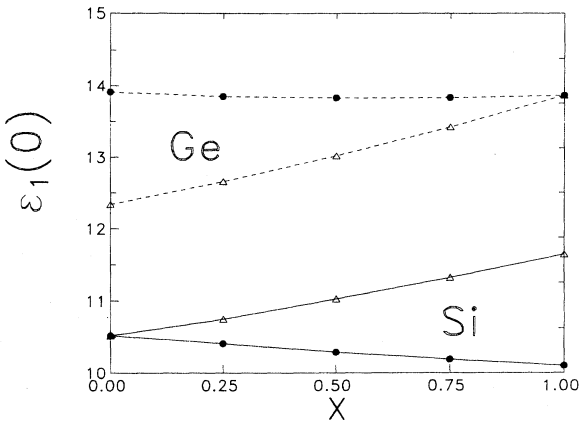

FIG. 12. Static dielectric constant, $\varepsilon_1(0)$, for strained Si (solid lines) and strained Ge (dashed lines) coherently grown on a $Si_{1-x}Ge_x$ (111) substrate, as a function of x, for polarization parallel ($\triangle$) and perpendicular ($\bullet$) to the growth plane.

dielectric constant shows a slight variation with strain, while for polarization in the growth plane $\varepsilon_1(0)$ changes more drastically. In the latter case, it varies almost linearly with strain, increasing with strain for the case of s-Si and decreasing for the case of s-Ge.

V. CONCLUSIONS

The optical properties of strained Si and Ge, as well as their anisotropy, are of major physical interest for future applications. We have presented an investigation of the energy band structure and optical properties of strained Si and Ge, coherently grown on (111)- and (110)-oriented $Si_{1-x}Ge_x$ substrates. The calculations have been performed in the framework of an empirical tight-binding model.

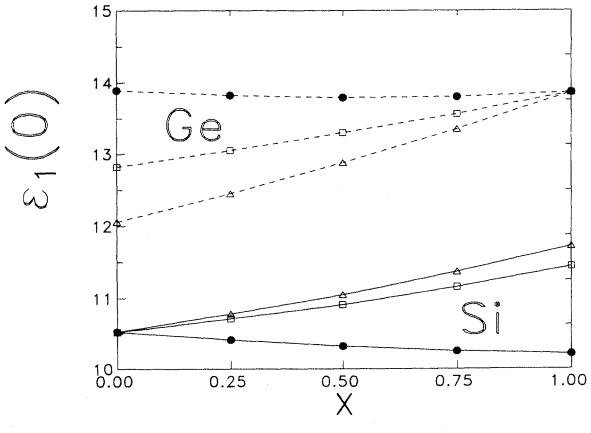

FIG. 13. Static dielectric constant, $\varepsilon_1(0)$, for strained Si (solid lines) and strained Ge (dashed lines) coherently grown on a $Si_{1-x}Ge_x$(110) substrate, as a function of x, for polarizations along (i) [$\bar{1}$10], (ε_1^{11}, ($\triangle$)), (ii) [001], (ε_1^{22}, ($\square$)), and (iii) [110], (ε_1^{33}, ($\bullet$)) directions.

The dependence of band-edge energies on strain and the direction of growth is presented and the calculated results are compared with those of the linear deformation potential theory. For strain along [111] and [110] directions, nonlinear effects becomes very important, especially for large strains. The fourfold lowest conduction-band state at the X point of the unstrained bulk BZ splits with strain into two twofold states. This nonlinear splitting produces a significant shift in the Δ conduction-band minima, not reproduced by the linear deformation potential theory. The ETB calculations predict that s-Si and s-Ge remain indirect gap semiconductors for both cases of strain and for all substrate compositions.

We have studied also the linear optical properties of (111)- and (110)-strained Si and Ge, calculating their dielectric tensors $[\varepsilon(\omega)]$. The optical anisotropy as well as the dependence of the several structures appearing in the ε_2 spectra on the strain has been investigated, and explained in terms of the band structure and transition probabilities. The anisotropy is quite large from the absorption edge up to the region of the E_2-like structure. For larger energies, the anisotropy almost diminishes.

Finally, we have calculated the static dielectric constant, ε_1 (0), for strained Si and Ge. The results show that for light polarization normal to the growth plane, $\varepsilon_1(0)$ changes slightly with strain for both directions of growth. For polarizations in the growth plane, the static dielectric constant depends in a sensitive way on the strain.

ACKNOWLEDGMENTS

This work has been supported in part by the ESPRIT Basic Research Action No. 7128, and the Greek Government Secretariat for Research and Technology.

* Electronic address: theodorou@olymp.ccf.auth.gr

[1] J.C. Bean, T.T. Sheng, L.C. Feldman, A.T. Fiory, and R.T. Lynch, Appl. Phys. Lett. **44**, 102 (1984).
[2] G. Abstreiter, H. Brugger, T. Wolf, H. Jorke, and H.J. Herzog, Phys. Rev. Lett. **54**, 2441 (1985).
[3] S.C. Jain, J.R. Willis, and R. Bullough, Adv. Phys. **39**, 127 (1990), and references therein.
[4] E. Kasper, H. Kibbel, H. Jorke, H. Brugger, E. Friess, and G. Abstreiter, Phys. Rev. B **38**, 3599 (1988).
[5] R. People, Phys. Rev. B **32**, 1405 (1985).
[6] G. Theodorou, P.C. Kelires, and C. Tserbak, Phys. Rev. B **50**, 18 355 (1994).
[7] M.M. Rieger and P. Vogl, Phys. Rev. B **48**, 14 276 (1993).
[8] Zhi-Zhong Xu, Phys. Rev. B **47**, 3642 (1993).
[9] M. Gell, Phys. Rev. B **41**, 7611 (1990).
[10] J.M. Hinckley and J. Singh, Phys. Rev. B **41**, 2912 (1990).
[11] Q.M. Ma, K.L. Wang, and J.N. Schulman, Phys. Rev. B **47**, 1936 (1993).
[12] C. Tserbak, H.M. Polatoglou, and G. Theodorou, Phys. Rev. B **47**, 7104 (1993).
[13] L. Kleinman, Phys. Rev. **128**, 2614 (1962).
[14] H. d'Amour, W. Denner, H. Schulz, and M. Cardona, J. Appl. Crystallagr. **15**, 148 (1982).
[15] C.S.G. Cousins, L. Gerward, J. Staun Olsen, B. Selsmark, and B.J. Sheldon, J. Appl. Crystallogr. **15**, 154 (1982).
[16] C.S.G. Cousins, L. Gerward, J. Staun Olsen, B. Selsmark, and B.J. Sheldon, J. Phys. **15**, 29 (1987).
[17] O.H. Nielsen and R.M. Martin, Phys. Rev. B **32**, 3792 (1985).
[18] J. Sanchez-Dehesa, C. Tejedor, and J.A. Verges, Phys. Rev. B **26**, 5960 (1982).
[19] C.S.G. Cousins, L. Gerwads, K. Nielsen, J. Staun Olsen, B. Selsmark, B.J. Sheldon, and G.E. Webster, J. Phys. C **15**, L651 (1982).
[20] F.H. Stillinger and T.A. Weber, Phys. Rev. B **31**, 5262 (1985).
[21] K. Ding and H.C. Andersen, Phys. Rev. B **34**, 6987 (1986).
[22] G.L. Bir and G.E. Pikus, *Symmetry and Strain-Induced Effects in Semiconductors* (Wiley, New York, 1974).
[23] L.D. Laude, F.H. Pollak, and M. Cardona, Phys. Rev. B **3**, 2623 (1971).
[24] I. Balslev, Phys. Rev. **143**, 636 (1966).
[25] C.G. Van de Walle and R.M. Martin, Phys. Rev. B **34**, 5621 (1986).
[26] M. Cardona and G. Harbeke, in *Physics of Group IV Elements and III-V Compounds*, edited by O. Madelund, H. Schulz, and K. Weiss, Landolt-Börnstein, New Series, Group. III, Vol. 17, Pt. a (Springer, Berlin, 1982).
[27] C. Tserbak and G. Theodorou, Phys. Rev. B **50**, 18 179 (1994).
[28] F. Wooten, *Optical Properties of Solids* (Academic, New York, 1972).